Astronomy & Astrophysics manuscript no. mgi˙i
February 17, 2015

Impact of new atomic data for NLTE studies of neutral magnesium in cool stars

I. Test cases with a simple Mg I model atom

T. Merle[1], F. Thévenin[2], N. Feautrier[3], O. Zatsarinny[4], M. Guitou[5], and A. Spielfiedel[3]

[1] Institut d'Astronomie et d'Astrophysique, Université Libre de Bruxelles, CP 226, Boulevard du Triomphe, 1050 Brussels, Belgium
[2] Université de Nice Sophia-Antipolis, Laboratoire Lagrange, UMR7293 CNRS, OCA, CS34229, F06304, Nice Cedex 4
[3] LERMA, Observatoire de Paris, 92195 Meudon Cedex, France
[4] Department of Physics and Astronomy, Drake University, Des Moines, IA 50311, USA
[5] Université Paris-Est, Laboratoire Modélisation et Simulation Multi-Echelle, MSME UMR 8208 CNRS, 5 Bd Descartes, Champs sur Marne, F-77454 Marne-la-Vallée, France

Received ?; accepted ?

ABSTRACT

Aims. We aim to calculate the non-LTE departure coefficients for the Mg I lines in benchmark stars based on the accurate quantum mechanical data for inelastic collisions of magnesium atoms with electrons and hydrogen atoms.
Methods. The method is based on the non-Local Thermodynamic Equilibrium (non-LTE) line formation using updated atomic data through the effective collision strengths for a simplified but consistent model atom of Mg I, especially for collisions with electrons and H atoms. In the present paper, only the levels for which we have new quantum mechanical H collision data are included in the model atom.
Results. Non-LTE departure coefficients for 7 Mg I lines of astrophysical interest are computed for four models corresponding to two dwarf and two giant stars as benchmark tests. The computations, including inelastic Mg+H collision data obtained by a quantum mechanical treatment, reduce the departures from LTE compared to neglecting Mg+H collisions (only free electron collisions) or using the classical Drawin's formula. The atomic data for inelastic collisions with hydrogen and electrons are provided in Appendix in terms of collision strengths.
Conclusions. The Mg+H charge exchange process is dominant in the formation of the resonance 2852 Å, the semi-allowed 4571 Å, and the b triplet (5167, 5172 and 5183 Å) lines in the atmospheres of these benchmark tests. The results concerning the IR 8806 and 11828 Å lines are more sensitive to the completeness of the model atom. Contrary to what is claimed in previous works, the use of the classical Drawin's formula has not to be considered as an upper limit toward the thermalization since we show for the main lines studied that the departure coefficients are closer to unity with the quantum mechanical collision data. Nevertheless, this study should be deepened with a carefull study of the impact of the completeness of the model atom of magnesium.

Key words. atomic data, atomic processes, line: formation, line: profile, Sun: abundances, stars: abundances

1. Introduction

The abundance of magnesium plays an important role in the study of the Galactic evolution (see, e.g., Gehren et al. 2006; Andrievsky et al. 2010) since it is an α-element produced by supernovæ of type II. It can be used as a reference element instead of iron to study the distribution of abundances of stellar populations (Cayrel et al. 2004; Fuhrmann 2008) although large scatters in [X/Mg] vs. [Mg/H] are found (Abia & Mashonkina 2004; Andrievsky et al. 2010); it also shows anti-correlation with aluminium in globular clusters (Gratton et al. 2001) and possibly with potassium (Mucciarelli et al. 2012, 2015). Moreover, Mg I lines can be observed even in ultra metal-poor stars (e.g. Norris et al. 2013).

A precise abundance determination of this element is then necessary to correctly interpret its numerous applications. The classical line formation synthesis suffers from the assumption of Local Thermodynamic Equilibrium (LTE). This approximation can lead to erroneous abundance determination for minority species, in particular for evolved and metal-poor stars (see Asplund 2005, for a review). Nevertheless, it is a difficult task to lift this approximation since a huge amount of atomic data for radiative and collisional transition probabilities are needed.

The first studies dedicated to the non-LTE effects on magnesium started with Athay & Canfield (1969) and Mauas et al. (1988) to constrain the microturbulence and the chromosphere profiles for the Sun. Then, numerous authors developed increasingly realistic Mg model atoms applied for the study of the Sun (Carlsson et al. 1992; Zhao et al. 1998), for hot (Gigas 1988; Przybilla et al. 2001) and cool (Zhao & Gehren 2000; Idiart & Thévenin 2000) stars. For convenience, non-LTE abundance corrections Δ[Mg/H] or non-LTE equivalent width corrections W/W^* were computed (Mashonkina et al. 1996; Shimanskaya et al. 2000; Zhao & Gehren 2000; Merle et al. 2011; Mashonkina 2013).

However, the main source of uncertainty for non-LTE stellar abundance analyses is the treatment of inelastic collisions with hydrogen atoms (see, e.g., Mashonkina 1996; Barklem et al. 2011). Until recently, the collisions with H atoms in late-type stars have been either neglected or treated with the so-called "Drawin's formula" (Drawin 1969), a modified version of

Table 1. Atmospheric parameters of the interpolated MARCS model atmospheres used. Reference solar values are A(Fe) = 7.45 and A(Mg) = 7.53.

Model	Star	$T_{\rm eff}$	$\log g$	[Fe/H]	[α/Fe]	ξ	geom.
1	Sun	5777	4.44	+0.00	+0.00	1	pp
2	HD 84937	6275	4.11	−2.20	+0.40	1	pp
3	Arcturus	4247	1.59	−0.50	+0.20	2	sph[a]
4	HD 122563	4587	1.61	−2.75	+0.40	2	sph[a]

[(a)] with $1 M_{\odot}$

the classical Thomson formula for ionization of atomic species by electron impact. This recipe was first applied to lithium (Steenbock & Holweger 1984), and then used by many authors due to the lack of experimental and theoretical data (see, e.g., Lambert 1993). However, a fudge factor $S_{\rm H}$ was introduced to scale the Drawin's formula depending on the element treated out of LTE. For instance, Shimanskaya et al. (2000) suggested for Mg I to use $0.5 \leq S_{\rm H} \leq 1$ whereas Gehren et al. (2004) determined $S_{\rm H} = 0.05$ based on analyses of nearby metal-poor star and the Sun. More recently, Sundqvist et al. (2008) used $S_{\rm H} = 0.001$ based on solar observations which lead to neglect H collisions especially in the red giant stars they studied. It was recently shown by Barklem et al. (2011) that the Drawin's formula compares poorly with the results of available full quantum scattering calculations based on detailed quantum mechanical studies. The Drawin's formula does not have a correct physical background. The formula significantly overestimates the rate coefficients for optically allowed transitions by an amount which varies with the transition (up to 7 orders of magnitude), and underestimates inelastic rates for optically forbidden transitions and charge exchange processes providing zero instead of nonzero values. In this situation, scaling factors do not solve these problems. Thus, nowadays it is well established that the Drawin's formula cannot be used for inelastic rate coefficients for low-energy atomic collision processes.

Recently, detailed quantum mechanical studies have been performed and accurate quantum cross-sections have been calculated for inelastic collisions of hydrogen atoms with light elements (Li I: Belyaev & Barklem 2003; Na I: Belyaev et al. 1999, 2010; Mg I: Guitou et al. 2011; Belyaev et al. 2012, and Al I: Belyaev 2013a). These quantum cross-sections have then been used to compute rates for inelastic hydrogen collisions with Li I (Barklem et al. 2003), Na I (Barklem et al. 2010), Mg I (Barklem et al. 2012), and Al I (Belyaev 2013). These computations were applied in atmospheres of late-type stars to determine non-LTE abundance corrections for Li I (Barklem et al. 2003; Lind et al. 2009) and Na I (Lind et al. 2011). They showed that charge exchange processes dominated compared to H collisions for excitation/de-excitation among low-lying levels; and this has a significant impact in determining the abundance corrections for Li I but not for Na I.

With the computations of accurate potentials for the MgH system (Guitou et al. 2010, 2011), quantum cross-sections in Mg + H collisions (Belyaev et al. 2012) and corresponding collision rate coefficients (Barklem et al. 2012), it is now possible to explore the role of inelastic collisions of neutral magnesium atoms with hydrogen atoms in late-type stars. In this article, we present new non-LTE departure coefficients concerning 7 Mg I lines in model atmospheres of two dwarf and two giant stars which correspond to four well known stars (the Sun, HD84937, Arcturus and HD122563 respectively).

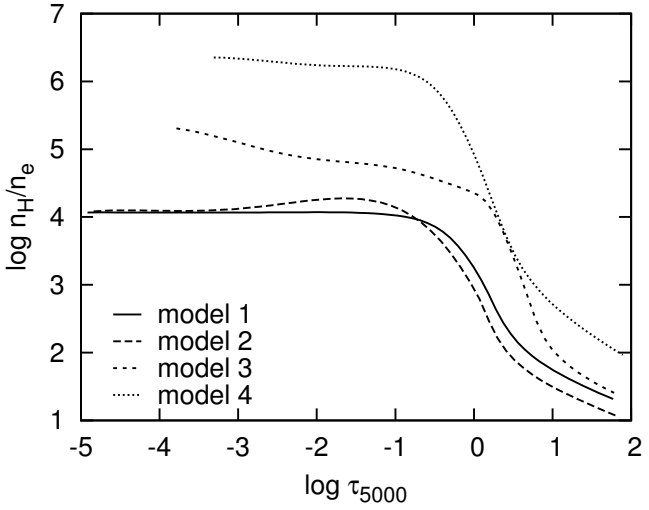

Fig. 1. Hydrogen to electron population density number ratio as the function of the standard optical depth in the MARCS model atmospheres of four benchmark stars.

The structure of the paper is as follows: the model atmospheres selected for the benchmark tests are described in Sect. 2. The simple Mg I model atom is described in Sect. 3 as well as the inelastic collision formulæ. Results and discussion are presented in Sect. 4 and 5.

2. Model atmospheres for benchmark tests

For this study, we selected four model atmospheres which correspond to four well known stars: (1) the Sun , (2) HD 84937 as a metal-poor main sequence turn-off halo star, (3) Arcturus as the well studied giant at sub-solar metallicity and (4) HD 122563 as a cool metal-poor field giant. They correspond to four different groups of stars to study the chemical evolution of the Galaxy.

The model atmospheres of the four benchmark tests are interpolated[1] (excepted for the solar one) in the MARCS database (Gustafsson et al. 2008). We used the parameters given in Table 1. The enhancement of α-element follows the Galactic one. Spherical models are used for the giants. The microturbulent velocity ξ is classically taken to 1 km s^{-1} in dwarfs and 2 km s^{-1} in giants.

While collisions with neutral hydrogen atoms are not important in hot stars, they can have a great impact in cool stars and especially in metal-poor giant stars. In the solar model, the hydrogen population density number is three orders of magnitude larger than the electron one where the continuum is formed and this can reach five orders of magnitude in the metal-poor giant model 4 as shown in Fig. 1. Even if the collision cross-sections with hydrogen are lower than the ones with electron by several orders of magnitudes, the impact of H collisions is non-negligeable.

3. Atomic data for Mg I

To assess the impact of the new atomic data on the statistical equilibrium, we decided to build a simplified model atom including only energy levels for which we have accurate quantum mechanical data for collisions with hydrogen atoms. The model

[1] using the Masseron code, available at: `http://marcs.astro.uu.se/software.php`

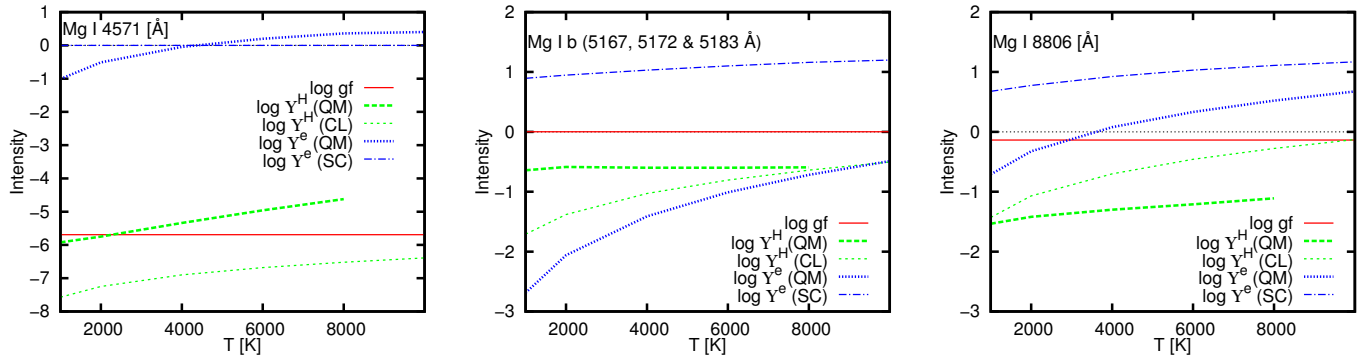

Fig. 2. Comparison of oscillator/collision strengths for the 4571 Å intercombination line (left), the b triplet (middle) and the 8806 Å line (right). Quantum mechanical (QM) cross-sections and rate coefficients are used for effective collision strengths with electrons $\Upsilon^{\rm e}_{ij}$ from Zatsarinny et al. (2009) and with neutral hydrogen $\Upsilon^{\rm H}_{ij}$ from Belyaev et al. (2012); Barklem et al. (2012). Semi-classical (SC) formulae are used for effective collision strengths with electrons $\Upsilon^{\rm e}_{ij}$ from Seaton (1962a) and the classical (CL) Drawin's formula for collisions with neutral hydrogen $\Upsilon^{\rm H}_{ij}$ from Drawin (1969).

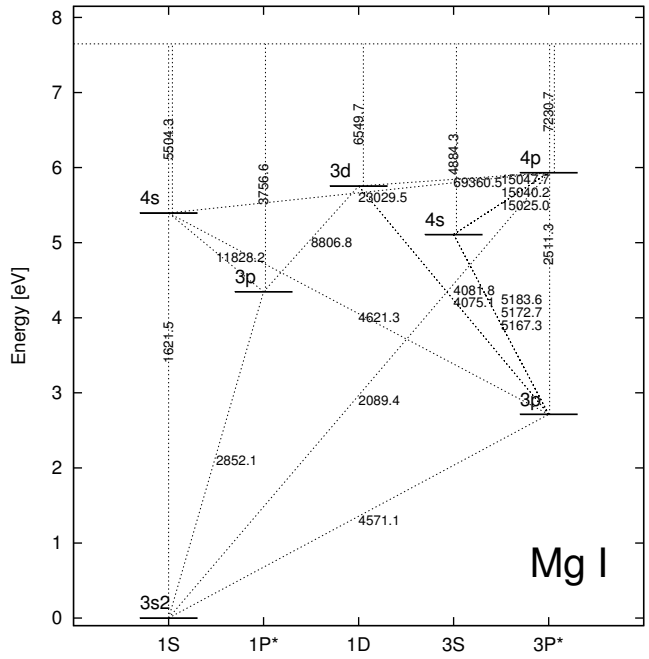

Fig. 3. Grotrian diagram of the Mg I model atom used in this work. Radiative bound-bound transition wavelengths and bound-free at the threshold transitions are labeled in Å.

includes the first seven low-lying levels plus the continuum. Two of the levels have a multiplicity of 3 (the metastable level 3s3p ^{3}P° and the level 3s4p ^{3}P°). A corresponding mean level is obtained from the average of fine structure levels weighted by their statistical weight. Grotrian diagram of this model is shown in Fig. 3.

The mean level population densities can deviate from LTE but the fine levels within a spectroscopic term are populated according to the LTE assumption. This is justified by the fact that the maximum difference in energy between fine levels of the 3s3p ^{3}P° is lower than 0.005 eV; such fine levels are therefore strongly coupled by collisions in atmospheres of the benchmark stars studied here where $0.37 \leq kT_{\rm eff} \leq 0.50$ eV. We are aware that the low number of included levels can give an incomplete picture of all the relevant processes in the model atom but including more levels with no reliable treatment of inelastic collisions can also lead to more complex results to understand with higher uncertainties (see discussion on the impact of the completeness of the model atom in Sect. 5.2).

3.1. Radiative data

The oscillator strengths f_{ij} are from the VALD database Kupka et al. (2000) except for the Mg I b triplet at 5167, 5172 and 5183 Å for which we used Aldenius et al. (2007) data, the 8806 and 11828 Å lines for which we used NIST data with excellent accuracy. Photoionization cross-sections are from TOPBASE with the same treatment as in Merle et al. (2011) to reduce the resolution keeping detailed of strong resonances near the photoionization threshold. Number of frequencies and wavelength range for each line are carefully chosen, especially for the very strong resonance line at 2852 Å which forms over more than 100 Å in Arcturus. The broadening parameters are the same as those used in Merle et al. (2011).

3.2. Collisional data

We give a special care to the treatment of collisions with electrons and H atoms. Firstly, we present the general relations of rates and effective collision strengths. Secondly, we present the quantum mechanical (QM) rates and the semi-classical (SC) approach of Seaton (1962a) for electrons and the classical (CL) Drawin's formula (Drawin 1969) for H-atoms. For electron collisions, we used the QM data in the model atom, but the SC data is also provided to do comparisons in term of effective collision strengths (see Sect. 3.3). Although we know that the Drawin's formula gives wrong results, we performed some calculations by means of the Drawin's formula as well, in addition to the use of QM data for collisions with H. We do this in order to show that the results based on the Drawin's formula deviate substantially from the results obtained with the QM data. We emphasize that any agreement between these results is occasional and does not prove usage of the Drawin's formula even with a scaling factor $S_{\rm H}$.

The collisional rates C_{ij} from state i to state j are the product of the density n_P of the collisional partner P with the rate coefficients R_{ij}:

$$C_{ij} = n_P R_{ij} \tag{1}$$

where R_{ij} are the Boltzmann thermal averages at temperature T of state-to-state inelastic Q_{ij} cross-sections:

$$R_{ij} = \left(\frac{8kT}{\pi\mu}\right)^{\frac{1}{2}} \left(\frac{1}{kT}\right)^2 \times \int_0^\infty Q_{ij}(E_\mathrm{c}) E_\mathrm{c} e^{-E_\mathrm{c}/kT} dE_\mathrm{c} \tag{2}$$

where k is the Boltzmann constant, E_c is the kinetic collision energy, μ is the reduced mass of the collision partners ($\mu \approx m_\mathrm{e}$ for electrons and $\mu \approx m_\mathrm{H}$ for hydrogen atoms). Rate coefficients obey the detailed balance relations.

For convenience, we convert collisional data to effective collisional strengths Υ_{ij}. The benefit of the use of this dimensionless variable Υ is its symmetry ($\Upsilon_{ij} = \Upsilon_{ji}$) with respect to the transition and the possibility to directly compare it with gf values. In terms of excitation cross-sections, Υ_{ij} is expressed as:

$$\Upsilon_{ij} = g_i \frac{kT}{E_\mathrm{H}^\infty} \int_0^\infty \sigma_{ij}(x)(x + x_{ij})\mathrm{e}^{-x}\mathrm{d}x \tag{3}$$

where g_i is the statistical weight of the lower level, E_H^∞ is the Rydberg unit of energy, $x = E/kT$ and $x_{ij} = E_{ij}/kT$ are the kinetic energy after excitation and the energy of the transition in unit of kT. σ_{ij} is the cross-section expressed in unit of πa_0^2 (a_0 is the Bohr radius). Thus the collision rate can be written as:

$$C_{ij} = n_P \, \mathcal{A} \, \frac{\Upsilon_{ij}(T)}{g_i \sqrt{T}} \mathrm{e}^{-E_{ij}/kT} \quad [\mathrm{s}^{-1}] \tag{4}$$

with:

$$\mathcal{A} = \pi a_0^2 \left[\frac{8E_\mathrm{H}^\infty}{\pi\mu}\right]^{1/2} \left[\frac{E_\mathrm{H}^\infty}{k}\right]^{1/2} [\mathrm{cm}^3 \ \mathrm{s}^{-1} \ \mathrm{K}^{1/2}], \tag{5}$$

where:

$$\mathcal{A} = \begin{cases} 8.629 \times 10^{-6} & \text{for electrons} \\ 2.014 \times 10^{-7} & \text{for H atoms.} \end{cases} \tag{6}$$

3.2.1. Quantum collision rates (QM)

For electrons, the QM approach is based on the R-matrix close coupling method (Zatsarinny et al. 2009). For 2 transitions for which QM cross-sections are not available, we used semi-classical data from Mauas et al. (1988) converted to effective collision strengths: for the triplet rising between 4s ^{3}S° – 4p ^{3}P° and for the forbidden transition 3p ^{3}P° – 4p ^{3}P°.

Rate coefficients for inelastic Mg+H collisions were calculated for all transitions between the lowest seven levels of Mg and the ionic state Mg$^+$(3s ^{2}S)+H$^-$(charge transfer). Those coefficients are based on cross-sections from full quantum scattering calculations based on quantum-chemistry descriptions of the relevant quasi-molecules. In the QM approach, the effective collision strengths with H atoms Υ_{ij}^H are given by:

$$\Upsilon_{ij}^\mathrm{H} = \mathcal{A}^{-1} g_j \sqrt{T} \, R_{ji} = 4.965 \times 10^6 g_j \sqrt{T} \, R_{ji} \tag{7}$$

where R_{ji} is the downward rate coefficient, in units of cm^3 s^{-1}, computed for the transitions between the seven lowest states of Mg I by Barklem et al. (2012).

Ionization of Mg I atom by H impact is dominated by the charge exchange (ion-pair production) process – at least for the low-lying levels. The upward (*ic* from the Mg level i to the ionic Mg$^+$(3s ^{2}S)+H$^-$ state c) and downward (*ci*) rates (for the mutual neutralization processes) as functions of H and H$^-$ densities (LTE values) are determined in detailed collision balance:

$$C_{ic}^\mathrm{H} = 2.014 \times 10^{-7} \, n_\mathrm{H}^* \frac{\Upsilon_{\mathrm{ci}}^\mathrm{H}}{g_i \sqrt{T}} \mathrm{e}^{-E_\mathrm{ic}/kT} \quad [\mathrm{s}^{-1}] \tag{8}$$

$$C_{ci}^\mathrm{H} = 2.014 \times 10^{-7} \, n_{\mathrm{H}^-}^* \frac{\Upsilon_{\mathrm{ci}}^\mathrm{H}}{g_c \sqrt{T}} \quad [\mathrm{s}^{-1}] \tag{9}$$

where $(E_\mathrm{ic} = E_i^\infty - 0.754)$ [eV] is the energy difference between the ionisation energy E_i^∞ of state i and the binding energy of H$^-$ compared to H, $g_c = 1$ is the statistical weight of the ionic (Mg$^+$(3s ^{2}S)+H$^-$) state and $\Upsilon_{\mathrm{ci}}^\mathrm{H}$ the effective collision strength for the downward charge exchange process to state i defined by:

$$\Upsilon_{\mathrm{ci}}^\mathrm{H} = 4.965 \times 10^6 g_c \sqrt{T} R_{ci} \tag{10}$$

where the R_{ci} (downward rate coefficient from ionic Mg$^+$(3s ^{2}S)+H$^-$ state to Mg$_i$ +H state) is tabulated as function of the temperature in Barklem et al. (2012). The QM effective collision strengths with electrons and H atoms are given in Appendix A and Appendix B respectively.

3.2.2. Semi-classical (SC) and classical (CL) collision rates

The SC approach to treat inelastic collisions with free electrons is based on the modified impact parameter method (Seaton 1962a) which requires the solution of an implicit equation with second kind Bessel functions and the oscillator strength of the transition. If the transition is radiatively forbidden, a collision strength of one is used by default. For ionisation by electrons, a SC expression using the pending photoionization cross-section at the threshold is used (Seaton 1962b).

The effective bound-bound collision strength with electrons Υ_{ij}^e, computed within the SC approach of (Seaton 1962a) is expressed as:

$$\Upsilon_{ij}^\mathrm{e}(T) = g_i \frac{kT}{E_\mathrm{H}^\infty} \int_0^\infty \min\left[\sigma_{ij}^0(x), \sigma_{ij}^1(x)\right](x + x_{ij})\mathrm{e}^{-x}\mathrm{d}x \tag{11}$$

where g_i, E_H^∞, x and x_{ij} have the same meaning as in Eq. 3. σ_{ij}^0 and σ_{ij}^1 are the cross-sections for collisions with electrons expressed in units of πa_0^2 (a_0 being the Bohr radius). σ_{ij}^0 is linked to the weak coupling and trivial to compute and σ_{ij}^1 corresponds to the strong coupling and needs the solution of an implicit equation (see Seaton 1962a and Merle 2012 for details).

For electron-ionisation, we can also define an effective collision strength as a function of the photoionization cross-section at the threshold σ_{ic}^rad in units of πa_0^2:

$$\Upsilon_{ic}^\mathrm{e} = \frac{2}{\alpha_\mathrm{FS}\sqrt{3}} g_i \frac{\sigma_{ic}^\mathrm{rad}}{x_{ij}} \langle g_\mathrm{bf}^\mathrm{e} \rangle \tag{12}$$

where α_FS is the fine structure constant and $\langle g_\mathrm{bf}^\mathrm{e} \rangle$ the effective bound-free Gaunt factor taken equal to 0.1 for neutral species (see Seaton 1962b for details).

Although we know that the classical Drawin's formula does not contain the relevant physics nor provide order-of-magnitude estimates of the collision rates coefficients (Barklem et al. 2011),

Table 2. Examples of QM to CL effective collision strengths ratio at $T = 6000$ K (scaling factor $S_{\rm H}$).

λ [Å]	$\frac{\Upsilon^{\rm H}_{ij}({\rm QM})}{\Upsilon^{\rm H}_{ij}({\rm CL})}$ $(= S_{\rm H})$	
2852.13	2.3×10^{-4}	
5167.32	2.24	1.60 for the triplet
5172.68	1.55	
5183.60	1.57	
8806.75	0.18	
11828.2	0.32	

we performed calculations by means of this formula for comparison, as it is still widely applied to simulate H-collisions processes in stars modeling. We emphasize that any agreement between these results is occasional and does not prove usage of the Drawin's formula even with scaling factors.

The effective Mg bound-bound collision strength with H atoms $\Upsilon^{\rm H}_{ij}$ is given in the CL approach by the Drawin's formula[2] (Drawin 1969) by:

$$\Upsilon^{\rm H}_{ij} = 4\sqrt{2}\,\frac{m_{\rm e}(m_{\rm H}+m_{\rm Mg})}{m_{\rm H}(m_{\rm H}+m_{\rm e})}\,g_i f_{ij}\,\frac{E^{\infty}_{\rm H}}{E_{ij}}\,\frac{1+2/x_{ij}}{x_{ij}} \tag{13}$$

where $m_{\rm e}$, $m_{\rm H}$ and $m_{\rm Mg}$ are the electron, hydrogen and magnesium masses, respectively. In this Drawin's formulation of H collisions, we used relation (13) with $f_{ij} = f_{ic} = 1$ by default for ionisation by H collisions but this must not to be compared with the Mg+H charge exchange process which requires less energy than pure ionization by H impact.

The SC and CL effective collision strengths with electrons and hydrogen atoms are given in Appendix A and Appendix B respectively.

3.3. Comparison of collision data with e^- and H atoms

Once collision data have been converted to effective collision strengths, we can compare them together with the oscillator strengths. We give illustrative examples in Fig. 2 for the 4571 Å intercombination semi-allowed, the b triplet and the 8806 Å lines.

For the intercombination semi-allowed 4571 Å line, the oscillator strength is extremely low compared with the electronic collision strength. When we compare QM $\Upsilon^{\rm e}_{ij}$ with the default value $\Upsilon^{\rm e}_{ij} = 1$ for forbidden transitions, we see a good agreement around $T = 4500$ K. However, if we had used SC from Seaton (1962a) based on the very low f-value, we would have obtained $\Upsilon^{\rm e}_{ij} = 1.15 \times 10^{-5}$ at this same temperature. Notice the large difference, about 2 orders of magnitude between CL and QM $\Upsilon^{\rm H}_{ij}$.

The strengths for the b triplet are given for the multiplet. The discrepancies between SC/CL and QM approaches are more pronounced for the electron than for the hydrogen collisions. At $T = 8000$ K collision strengths are, by coincidence, in good agreement for collisions with H and of the same magnitude compared with QM $\Upsilon^{\rm e}_{ij}$. The QM $\Upsilon^{\rm e}_{ij}$ is at least 2 orders of magnitude lower than SC $\Upsilon^{\rm e}_{ij}$ leading to too strong collision rates for this multiplet with SC prescription.

[2] using the version of Lambert (1993), equation (A10)

For illustrative purpose, the ratio between QM and CL $\Upsilon^{\rm H}_{ij}$ (scaling factor $S_{\rm H}$) is given at $T = 6000$ K in Table 2. For the line at 8806 Å, the CL $\Upsilon^{\rm H}_{ij}$ overestimates the QM $\Upsilon^{\rm H}_{ij}$ by about one order of magnitude. This leads at $T = 6000$ K to a scaling factor $S_{\rm H} = \Upsilon^{\rm H}_{ij}({\rm QM})/\Upsilon^{\rm H}_{ij}({\rm CL}) = 0.18$. For other transitions, the CL rate coefficients may overestimate the QM ones by several orders of magnitude (e.g. the 2852 Å line) or significantly underestimate some QM rate coefficients, mainly for optically forbidden transitions (see Appendix B).

4. Results

To compute the departure coefficients of Mg I, we used the 1D non-LTE radiative transfer code MULTI2.2 (Carlsson 1986) which has been modified to treat inelastic collisions with electrons and hydrogen atoms. Line blanketing effect is taken into account through the inclusion of background atomic lines of other main species.

We present new non-LTE calculations accounting for inelastic collisions with free electrons and H atoms from quantum mechanics (QM) calculations. We focused on four benchmark test: two dwarfs and two red giants with solar and low metallicities. In addition, we present results of test calculations obtained with different input data.

The departure coefficients $b_i = n_i/n^*_i$ (ratio between non-LTE over LTE number population densities of level i) in the atmospheres of these stars are given in Fig. 4. As expected, when collisions with H are taken into account (left and middle panels), the departure coefficients of Mg I are reduced compared with pure e^- collisions in the four model atmospheres and remain lower than one. This is due to the over-ionization of Mg I by the UV radiation of non-local origin coming from deeper layers. The Mg II population density is in LTE except in Arcturus where the effective temperature is sufficiently low to allow Mg I ionization fraction to be as large as Mg II below $\log \tau_{5000} = -2$. Nevertheless, the departure coefficients are less reduced when the CL input data are used instead of the accurate QM data.

When no H collisions are considered (right panels of Fig. 4), the populations diverge from LTE for $\log \tau_{5000} \leq 0.2$ in the dwarves (2 upper panels) and for $\log \tau \leq 0.5$ in the giants (2 lower panels). If CL H collisions are included (middle panels of Fig. 4), the populations diverge from LTE approximately at the same optical depths but share the same departure coefficients from LTE until $\log \tau_{5000} \approx -0.5$ (except for the ionization stage). If the lines form at this optical depth or deeper, the non-LTE line source functions are very close to the Planck function, assuming that $S_{ij}/B_{ij} = b_j/b_i$ (Wien regime), but the line opacities are still possibly reduced ($b_i < 1$) leading to weaker lines compared with LTE. If QM collisions are used instead of CL ones (left panels of Fig. 4), the departure coefficients are close to LTE until $\log \tau_{5000} \approx -1$ except for the ground stage in HD 122563.

Contrary to a spread idea that the CL Drawin's formula gives an upper limit to the expected departure coefficients, we show that usage of the QM data for Mg+H collisions produces number densities for Mg I which are more thermalized compared with the CL formula, even with $S_{\rm H} = 1$. This will produce smaller non-LTE abundance corrections.

Indeed, the ion-pair production and mutual neutralization processes play a main role in this assertion. To better understand how, we computed the departure coefficients excluding these processes and compared with previous results. We plot the $\Delta b/b_{\rm ref}$ where the departure coefficients $b_{\rm ref}$ are related to a model atom without H collisions for the solar model. This in-

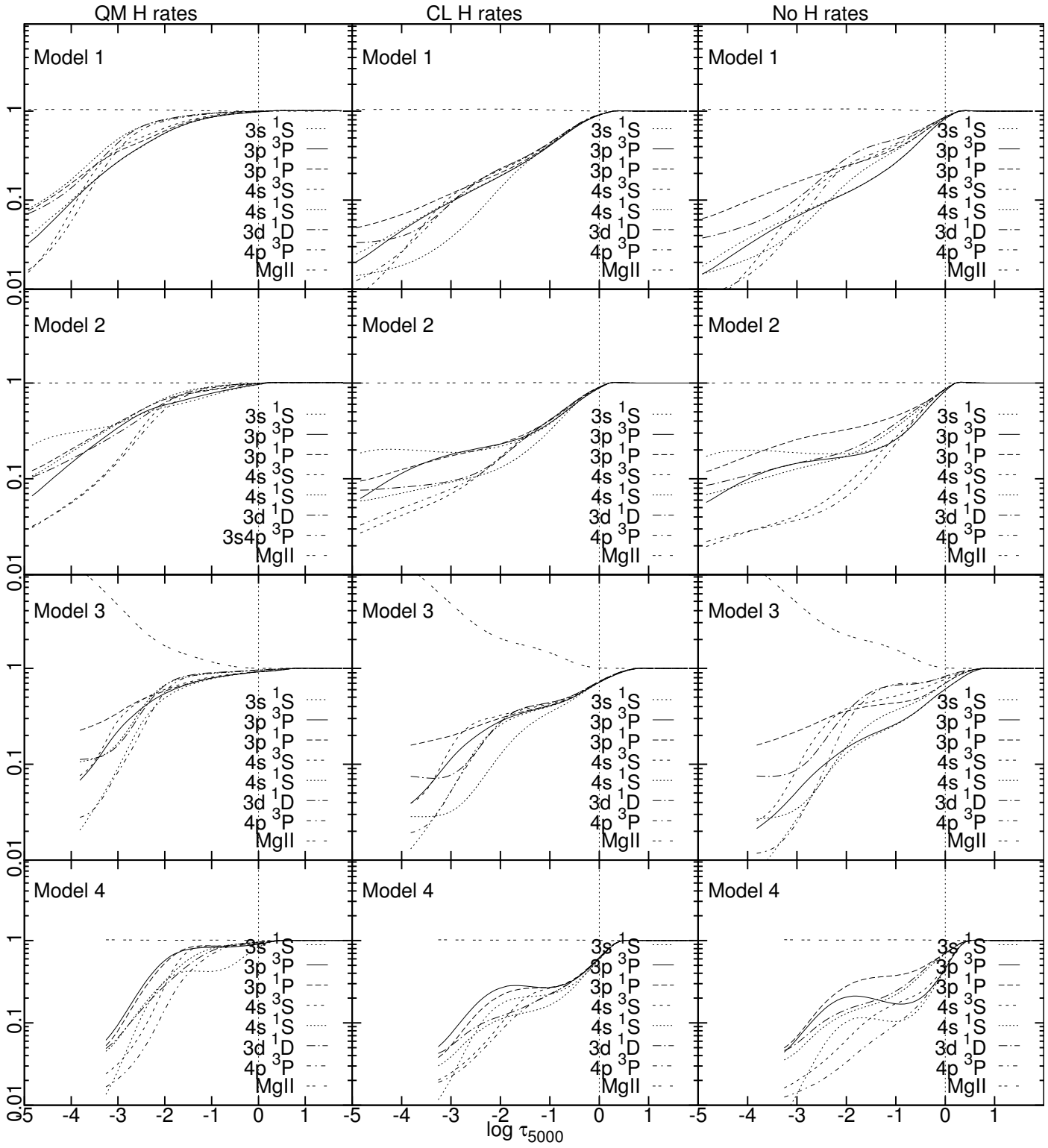

Fig. 4. The Mg I departure coefficients b_i as a function of the continuum optical depth at 5000 Å for each model atmosphere (each row): using the QM calculations (left column); with inelastic collisions with H atoms using the (CL) Drawin's formula with $S_{\rm H} = 1$ (center column) and without inelastic collisions with H atoms, i.e. pure QM e^- collisions (right column). The departure coefficients of the Mg I levels are labeled omitting the 3s electron.

λ [Å]	W^* [mÅ]	W/W^*(QM H rates)	W/W^*(CL H rates)	W/W^*(No H rates)
Model 1	($T_{\rm eff}$ = 5777 K, $\log g$ = 4.44, [Fe/H] = 0.00, A^*(Mg) = 7.53)			
2852.13	22653	0.95	0.82	0.73
4571.09	101	0.95	0.87	0.83
5167.32	788	0.96	0.85	0.72
5172.68	1344	0.96	0.85	0.71
5183.60	1713	0.96	0.85	0.71
8806.75	523	0.92	0.86	0.83
11828.2	815	0.89	1.01	1.02
Model 2	($T_{\rm eff}$ = 6275 K, $\log g$ = 4.11, [Fe/H] = −2.20, [α/Fe] = +0.40, A^*(Mg) = 5.73)			
2852.13	1810	0.87	0.69	0.57
4571.09	5	0.73	0.43	0.33
5167.32	110	0.92	0.82	0.78
5172.68	154	0.94	0.85	0.81
5183.60	184	0.95	0.84	0.80
8806.75	82	0.91	0.78	1.05
11828.2	105	0.81	1.06	1.18
Model 3	($T_{\rm eff}$ = 4247 K, $\log g$ = 1.59, [Fe/H] = −0.50, [α/Fe] = +0.20, A^*(Mg) = 7.23)			
2852.13	153745	0.91	0.86	0.72
4571.09	227	0.94	0.93	0.92
5167.32	1011	0.96	0.90	0.75
5172.68	1718	0.96	0.90	0.74
5183.60	2187	0.96	0.90	0.74
8806.75	625	1.04	0.99	1.16
11828.2	875	1.04	1.17	1.28
Model 4	($T_{\rm eff}$ = 4587 K, $\log g$ = 1.61, [Fe/H] = −2.75, [α/Fe] = +0.40, A^*(Mg) = 5.18)			
2852.13	10172	0.64	0.63	0.30
4571.09	84	0.54	0.62	0.31
5167.32	184	1.02	0.92	0.84
5172.68	249	1.01	0.88	0.80
5183.60	295	1.00	0.86	0.76
8806.75	125	1.20	0.94	1.15
11828.2	155	1.15	1.17	1.26

Table 3. LTE equivalent widths (W^*) and non-LTE over LTE equivalent width ratios (W/W^*) of Mg I lines for different sets of H collisions (QM = Quantum Mechanics, and CL = Classical treatment with $S_{\rm H}$ = 1) for the 4 benchmark tests. W^* are given in mÅ.

creases the readability of the contributions of the CL and QM collision sets with H atoms to the departure coefficients. The left and right panels of Fig. 5 show, for the Sun, that the departure coefficients between CL and QM are completely different: if we exclude the ion-pair production and mutual neutralization processes, the change of departure coefficients are roughly similar in amplitudes and patterns (middle and right panels of Fig. 5). If we look in more details for ground state and first excited level (dotted and full lines), the Drawin approach gives larger contribution to the departure coefficients than the QM without the charge exchange processes within a factor of two. However, for the 4s ^{1}S level, the change in departure coefficient is opposite in sign. This is due to the fact that the H collision rates arising from this level are the strongest and produce populations with the smaller departure coefficients from LTE (see top left panel of Fig. 4). The charge exchange process gives positive change for all the coefficient which can reach a factor of 10 for the 4s ^{1}S level (left panel of Fig. 5). This explains why non-LTE effects are more reduced when taking into account QM collision data as compared with CL Drawin collision data.

The computed Mg I non-LTE over LTE equivalent width ratios W/W^* are given in Table 3 with the use of different treatments of the H-collisions: with the QM data (1$^{\rm st}$ column); with the CL Drawin's formula ($S_{\rm H}$ = 1, 2$^{\rm nd}$ column) and with no H collisions, i.e. pure QM electron collisions (3$^{\rm rd}$ column). A general view of the results shows that the W/W^* are mainly lower than one leading to positive non-LTE abundance corrections excepted for the near IR lines (8806 and 11828 Å) in giant models. When inelastic collisions with hydrogen are not taken into account, the W/W^* are mainly much lower than one even in giant models from which we would expect to have less impact of hydrogen collisions since these atmospheres are more diluted than in dwarf stars. These results show that this assumption is clearly not well suited for giant stars.

We illustrate the differences in the line formation with LTE assumption and without LTE but with different datasets for H collisions for the two metal-poor stars where the non-LTE effects are important. Focusing on the intercombination resonance line at 4571 Å in model 4, we show the departure coefficients of the

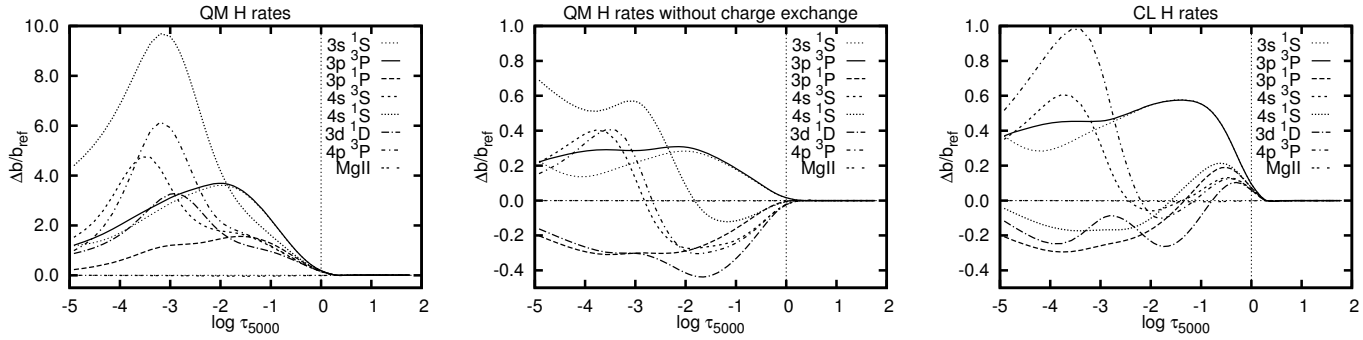

Fig. 5. Change of departure coefficients $\Delta b = b - b_{\rm ref}$ relative to model atom without H collision rates $b_{\rm ref}$ in the solar model (corresponding to the top right panel of Fig. 4). Left: for QM H collision rates. Middle: for the QM H collision rates excluding charge exchange processes. Right: for CL H collision rates (with $S_{\rm H} = 1$). The changes of departure coefficients of each level are labeled omitting the 3s electron.

levels involved in the transition, the source functions and the line profiles in Fig. 6. When no H collisions are included, the departure coefficient from LTE of the ground stage is reduced by a factor of 5 (left panel, the thickest black full line) at the line forming optical depth (showed by the red tick at $\log \tau_{5000} \approx -1.5$) and the S/B is the highest (middle panel). The reduction of the lower population and the increase of the source function act in the same way to reduce strongly the line strength (right panel, the thickest black full line) compared with LTE (right panel, blue short dashed line). The inclusion of the CL (green dashed lines) or the QM (red full line) H collisions leads to increase the line strength compared with no H collisions following the intensity of the S/B at the line forming optical depth.

For the b triplet, we show the departure coefficients of the levels involved in the transition, the source functions and the line profiles in Fig. 7 for model 2 where the non-LTE effects are the most important among the four benchmark tests. The upper departure coefficients become smaller than the lower one in the upper part of the model atmosphere. This relative change leads to source functions which are lower in the line core and larger in the wings than the Planck function explaining the shape of the different line profiles. The component at 5167.3 Å is the less affected by the non-LTE effect because it has the lowest $\log gf$ and forms deeper in the atmosphere at a position where the source function is close to one. With the QM H collisions, the non-LTE effects are weaker in the other benchmarks.

5. Discussion

5.1. Comparison with previous studies

We can compare our W/W^* (with no H collisions) for models 3 and 4 with Table 6 of our previous study (Merle et al. 2011) or online data (Merle et al. 2012) where we computed a grid of W/W^* for atmospheric parameters of (super)giant stars with a much more complete model atom but with less accurate atomic data for the treatment of inelastic collisions. For Arcturus, the comparison with the W/W^* retrieved for $T_{\rm eff} = 4250$ K, $\log g = 1.5$ and [Fe/H]$= -0.50$ on the grid are not very good. Two main reasons can explain the discrepancies. Firstly, for the b triplet, W/W^* of Merle et al. (2012) can be as large as 0.13 due to the fact that QM electronic collision strengths (used in the present study) are lower than the SC electronic collision strengths used in Merle et al. (2011) by more than 2 order of magnitudes at 4000 K, as can be seen on the middle panel of Fig. 2. Such impact of electronic data underlines the need to use QM data even for electron collision in the non-LTE approach. Secondly, concerning the 8806 and 11828 Å lines, the completeness of the model atom adds more discrepancy (until 0.22) to the previous reason. These 2 lines involved the highest levels of our simple model atom whereas a bunch of supplementary higher levels with many lines are used in Merle et al. (2011). The impact of the completeness, which will be also discussed in the following section, is all the more important as the fraction of neutral magnesium is not negligeable compared with the ionized stage due to the low effective temperature compared to the other studied stars. Thus, higher levels are comparatively more populated. On the contrary, good agreement in W/W^* are found for model 4 for which we compared with W/W^* retrieved for $T_{\rm eff} = 4500$ K, $\log g = 1.5$ and [Fe/H]$= -2.50$. The differences are lower than 0.05. This can be explained by the fact that there are much less free electrons in this metal-poor star, then, the W/W^* are less sensitive to the different electronic datasets.

The recent study by Mashonkina (2013) focused on the Sun, A-type and metal-poor stars. We have 3 models in common corresponding to the Sun, HD 122563 and HD 84937 but we can compare departure coefficients only for HD 122563 (model 4). The departure coefficients from Figure 1 of Mashonkina (2013) correspond to the atmospheric parameters of HD 122563 (with and without QM H collisions) and can be compared with our departure coefficients for the our model 4 (Fig. 4, left and right bottom panels). Without H collisions (pure electronic collisions) we obtained similar patterns but with stronger general depletion due to our limited model atom. Indeed, the inclusion of more higher excited levels would tend to reduce the depopulation of the lower levels through a cascade ladder from the next ion reservoir. This trend is general for minority species as shown by Bruls et al. (1992). However, we can notice an appreciable difference for the ground stage, the 3p ^{3}P° and the 3p ^{1}P° levels. These levels are strongly coupled in Mashonkina (2013), whereas they are less coupled in our work. If we can assume that it could be possibly the case for the ground state and the 3p ^{3}P° level, however, it should not be the case for the ground state and the 3s ^{1}S level since they are linked by the very strong UV resonance line at 2852 Å which produces a strong divergence in our departure coefficients. Even for the ground state and the 3p ^{3}P° level, in this metal-poor star where the hydrogen density is 6 orders of magnitude larger than the electron density at the line forming region (Fig. 1), hydrogen collision rates compete with electron ones. From Fig. 2, left, we see that the oscillator strength is at

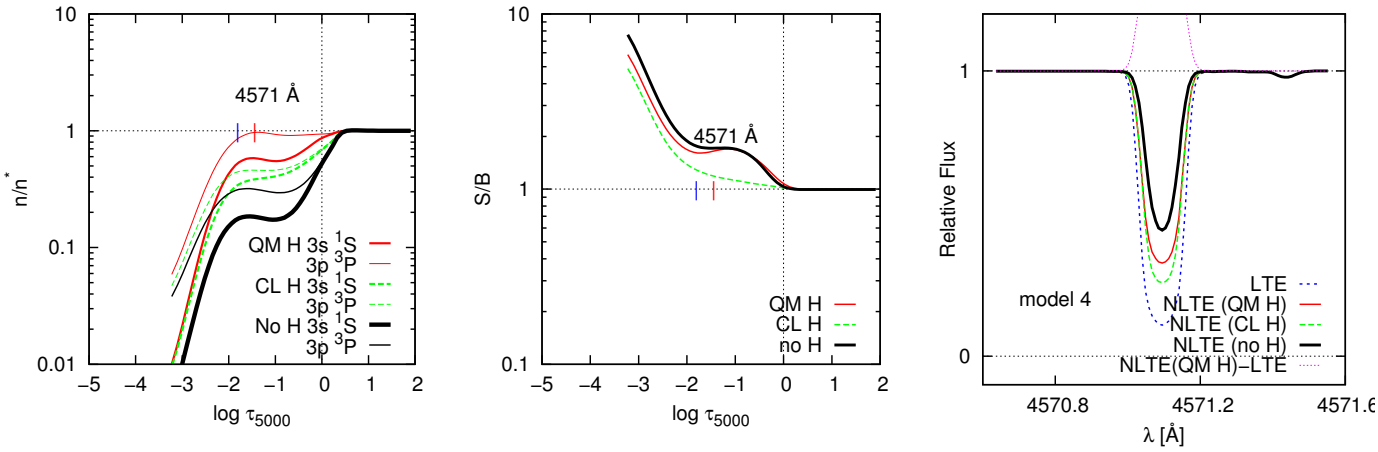

Fig. 6. Formation of the Mg I 4571 Å intercombination line in the model 4 (giant metal-poor). Left: departure coefficients of the levels implied in the line. Middle: line source function. Right: line profile. Vertical ticks show the optical depths where the line cores are formed in LTE (blue) and in non-LTE (red).

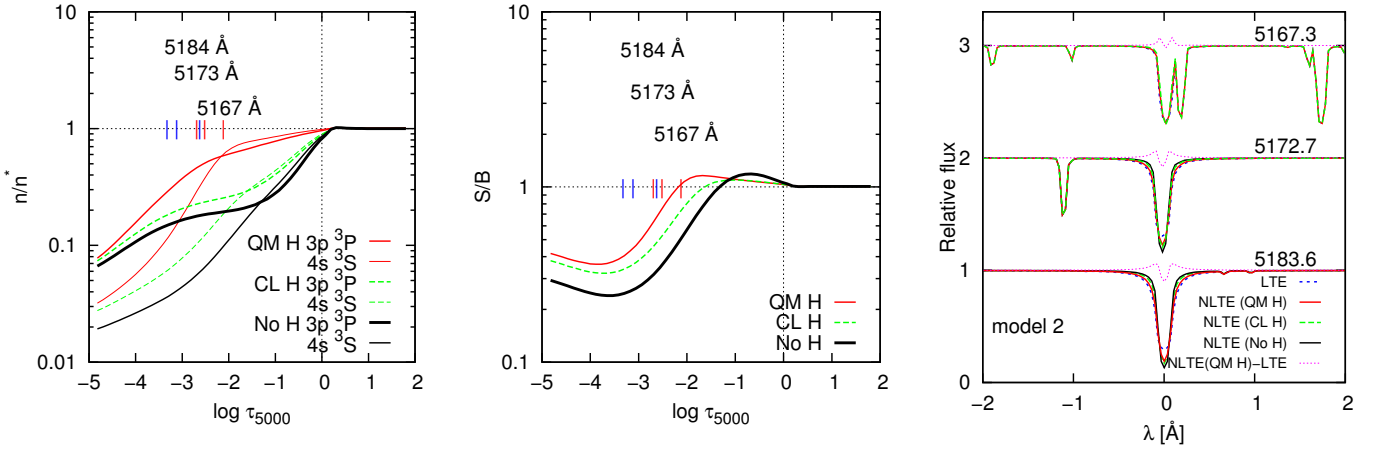

Fig. 7. Formation of the Mg I b triplet in the model 2 (dwarf metal-poor). Left: departure coefficients of the levels implied in the b triplet. Middle: line source function of the b triplet. Right: line profiles of the b triplet. Vertical ticks show the optical depths where the line cores are formed in LTE (blue) and in non-LTE (red).

the same order of magnitude as the effective collision strength with H. This implies that 3p ^{3}P° is not necessarely thermally coupled with the ground state since photon losses are not negligible compared with H collisions. If we compare departure coefficients including QM H collisions, we notice a main difference: Mashonkina (2013) found positive departure coefficients for the four low lying levels ($-2.5 \leq \log \tau_{5000} \leq -1$). On the contrary, we found that departure coefficients are strongly reduced and close to unity but not positive. This large difference could be due to a different treatment of the charge exchange since this process dominates over the Mg bound-bound H collisions for low-lying levels.

The results of Table 3 show the large influence of the QM Mg+H collision data for Mg compared with CL and no H collisions. Together with relative departure coefficients from Fig. 5, these show that charge transfer dominates the Mg+H/Mg$^+$+H$^-$ collisions rates compared to excitation/de-excitation Mg+H collision rates. Contrary to Na I (Lind et al. 2011), the QM Mg+H collision rates are larger compared with CL Mg+H collision rates (Drawin's formula). This implies that using the Drawin's formula will not necessarily give lower limits to the abundance corrections.

5.2. Impact of the completeness of the model atom

As specified in Sect. 3 we decided to focus on the coherence in atomic dataset used in the model atom rather than on the completeness of the model atom. In consequence, we did not compute any non-LTE abundance corrections in these models. To have an idea of the effect of the completeness of the model atom, we present a parameterization of the ground stage departure coefficient of Mg I with the number of included energy levels for the Sun in Fig. 8. Starting with a basic 2 level atom, including only the ground and first ionized stage of magnesium, we see that non-LTE only affects the upper part due to photoionisation of the ground stage (solid line). Including 3p ^{3}P° energy levels produces a large depletion of population due to large photoionization cross-sections of this level (long dashed line). Introduction of the 4s ^{3}S limits the depletion of the ground stage because it adds a channel for recombination toward de 3s ^{3}P° (short dashed line). With the addition of the 3p ^{1}P° we add a strong resonance line at 2852 Å that depletes directly the ground state by action of the UV radiation of non local origin (dotted line). Until the model with 8 levels, the population of the ground stage is strongly affected by the different levels, lines and continua.

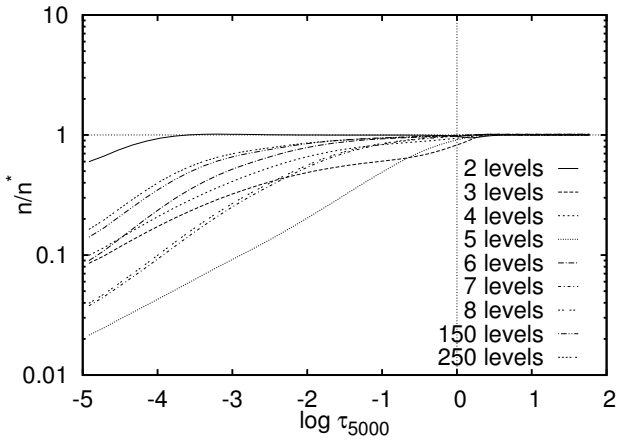

Fig. 8. Departure coefficient n/n^* of the ground stage $2p^6 3s^2\ ^1S$ of Mg I as a function of the optical depth for the solar MARCS model atmosphere, parametrized by the number of energy levels included in the model atom.

We also give the departure coefficient of the ground stage for the model atom with 150 levels (Merle et al. 2011) and for a model atom with 250 energy levels (including all levels with one excited electron from NIST). We see that between model with 8 levels and 150 levels, the depopulation is reduced by a factor of ~ 5 at the top of the model atmosphere whereas between 150 and 250 energy levels, the depopulation is only reduced by a factor of 1.2. This underlines the importance of the completeness of the model atom in terms of energy levels to obtain the right number population densities (see, e.g., Bergemann & Cescutti 2010). In the case of the ground stage of Mg I, the depopulation reduces with the increasing number of levels giving lower abundance corrections for lines related to this level and to levels strongly coupled to it. This explains why we do not provide any non-LTE abundance corrections to prevent effects due to the lack of completeness of model atom.

5.3. Uncertainties on collision data

Uncertainties on the collision data are known to be the weakness of the non-LTE treatment. That is the reason why we do not mention the impact on uncertainties of the oscillator strengths and energy levels. Impact of the completeness are mentionned in the previous sub-section. We focus on the uncertainties due to collisions with electrons and with H atoms.

Uncertainties on QM e^- collision strengths can be estimated only from comparison with experiment because no special convergence study has been done. It shows an uncertainty of about 10 % for strong transitions like $3s\ ^1S - 3p\ ^1P$ or $3s\ ^1S - 3d\ ^1D$, and of about 20 % for weak ones like $3s^{\ 1} - 4s\ ^1S$ (Zatsarinny et al. 2009). We applied a factor of 1.2 on e^- collision strengths as an upper limit and 0.8 as a lower one. We redid the entire calculations of the statistical equilibrium. The results showed that population densities are not really affected by uncertainties on e^- collisions except for the resonance line at 2852 Å and for the intercombination line at 4571 Å. The W/W^* differences are lower than 2 % in the models 1, 2 and 3. For the two resonance lines, the differences reach 7 % whereas they remain lower than 1 % for the other lines in model 4.

Uncertainties on QM Mg+H collision rates can be better estimated using the fluctuation factors computed by Barklem et al. (2012). Upper and lower values for the fluctuation factors are given for each transition: from 0.2 to 0.8 for lower values and from 1.2 to 6 for the upper ones. We applied them and computed again the statistical equilibrium. In the models 1 and 3 (the Sun and Arcturus), the W/W^* differences are of or lower than 2 %. Impact of uncertainties on H collisions is more important in metal-poor stars because the electron density dramatically decreases. The W/W^* differences are lower than 4 % for the b triplet but can reach 10 % for the 4571 Å line and even 15 % for the 11828 Å lines. These high uncertainties on W/W^* would lead to uncertainties in the abundance corrections of the order of 0.1 dex in the extreme cases.

If we neglect the charge exchange process, the W/W^* differences are largely increased in the way that increase the non-LTE effects. For the 4571 Å line, the increase is of 10 % and reaches almost 40 % in the model 2. In the model 3 the differences are less than 6 %. For the b triplet, the W/W^* is reduced by 6 % in this model and by in average 15 % in the other models. The neglect of the charge exchange process should lead to overestimate the positive non-LTE abundance corrections by amounts that can reach 0.2 dex for the b triplet.

6. Conclusions

This theoretical study is dedicated to the calculation of non-LTE Mg I line formation based on the new and accurate quantum-mechanical data for collisions of Mg I with electrons and hydrogen atoms. We used a simplified but consistent model atom of Mg I including all the levels and transitions for which we have quantum mechanical (QM) collision data. We compared them with the classical (CL) Drawin's formula for Mg+H collisions. We computed non-LTE departure coefficients with MULTI 2.2 for interpolated MARCS model atmospheres for 4 benchmark tests (the Sun, HD 84937, Arcturus and HD 122563).

We can draw several main conclusions: (i) Contrary to what is claimed in the literature, using the CL Drawin's formula overestimates corrections as compared with the accurate QM rates for inelastic collisions of Mg with H, even if the scaling factor is fixed to a high value ($S_H = 1$). (ii) The charge exchange plays a main role in the formation of the 2852 Å, 4571 Å and the b triplet lines while it is not the case for the 8806 Å and 11828 Å lines. (iii) As already underlined in numerous studies, impact of completeness of the model atom is very important to obtain the correct statistical equilibrium because adding levels toward the Mg II ionization stage with decreasing energy transitions reduces the underpopulation of Mg I levels and reduces the departures from LTE.

Both QM inelastic H collisions with charge exchange and completness of the model atom will reduce the departures from LTE. The grid computed by Merle et al. (2011) gives an upper limit of corrections that have to be lowered by QM collisions as it is shown in this study.

This study shows that more QM H collisions are needed for other α-elements to progress in the understanding of the galactic evolution through chemical tracers like magnesium, calcium or silicon. In that respect, new developments on the non-adiabatic nuclear dynamics applied to silicon (Belyaev et al. 2014) are very promising for treating H collisions in model atom with numerous levels.

Acknowledgements. The authors acknowledge the role of the SAM collaboration (`http://www.astro.uu.se/~ulrike/GaiaSAM`) in stimulating this research through regular workshops. TM is short term foreign postdoctoral fellow

from FNRS (FRFC convention, ref: PDR T.0198.13). AKB acknowledges financial support from the Russian Foundation for Basic Research (Grant No. 13-03-00163-a). This work has made use of the VALD database, operated at Uppsala University, the Institute of Astronomy RAS in Moscow, and the University of Vienna.

References

Abia, C. & Mashonkina, L. 2004, MNRAS, 350, 1127 1
Aldenius, M., Tanner, J. D., Johansson, S., Lundberg, H., & Ryan, S. G. 2007, A&A, 461, 767 3
Andrievsky, S. M., Spite, M., Korotin, S. A., et al. 2010, A&A, 509, A88 1
Asplund, M. 2005, ARA&A, 43, 481 1
Athay, R. G. & Canfield, R. C. 1969, ApJ, 156, 695 1
Barklem, P. S., Belyaev, A. K., & Asplund, M. 2003, A&A, 409, L1 2
Barklem, P. S., Belyaev, A. K., Dickinson, A. S., & Gadéa, F. X. 2010, A&A, 519, A20 2
Barklem, P. S., Belyaev, A. K., Guitou, M., et al. 2011, A&A, 530, A94 1, 2, 4
Barklem, P. S., Belyaev, A. K., Spielfiedel, A., Guitou, M., & Feautrier, N. 2012, A&A, 541, A80 2, 3, 4, 10, 13
Belyaev, A. K. 2013, A&A, 560, A60 2
Belyaev, A. K. 2013a, Phys. Rev. A, 88, 052704 2
Belyaev, A. K. & Barklem, P. S. 2003, Phys. Rev. A, 68, 062703 2
Belyaev, A. K., Barklem, P. S., Dickinson, A. S., & Gadéa, F. X. 2010, Phys. Rev. A, 81, 032706 2
Belyaev, A. K., Barklem, P. S., Spielfiedel, A., et al. 2012, Phys. Rev. A, 85, 032704 2, 3
Belyaev, A. K., Grosser, J., Hahne, J., & Menzel, T. 1999, Phys. Rev. A, 60, 2151 2
Belyaev, A. K., Yakovleva, S. A., & Barklem, P. S. 2014, A&A, 572, A103 10
Bergemann, M. & Cescutti, G. 2010, A&A, 522, A9 10
Bruls, J. H. M. J., Rutten, R. J., & Shchukina, N. G. 1992, A&A, 265, 237 8
Carlsson, M. 1986, Uppsala Astronomical Observatory Reports, 33 5
Carlsson, M., Rutten, R. J., & Shchukina, N. G. 1992, A&A, 253, 567 1
Cayrel, R., Depagne, E., Spite, M., et al. 2004, A&A, 416, 1117 1
Drawin, H. W. 1969, Zeitschrift fur Physik, 225, 483 1, 3, 5, 13
Fuhrmann, K. 2008, MNRAS, 384, 173 1
Gehren, T., Liang, Y. C., Shi, J. R., Zhang, H. W., & Zhao, G. 2004, A&A, 413, 1045 2
Gehren, T., Shi, J. R., Zhang, H. W., Zhao, G., & Korn, A. J. 2006, A&A, 451, 1065 1
Gigas, D. 1988, A&A, 192, 264 1
Gratton, R. G., Bonifacio, P., Bragaglia, A., et al. 2001, A&A, 369, 87 1
Guitou, M., Belyaev, A. K., Barklem, P. S., Spielfiedel, A., & Feautrier, N. 2011, Journal of Physics B Atomic Molecular Physics, 44, 035202 2
Guitou, M., Spielfiedel, A., & Feautrier, N. 2010, Chemical Physics Letters, 488, 145 2
Gustafsson, B., Edvardsson, B., Eriksson, K., et al. 2008, A&A, 486, 951 2
Idiart, T. & Thévenin, F. 2000, ApJ, 541, 207 1
Kupka, F. G., Ryabchikova, T. A., Piskunov, N. E., Stempels, H. C., & Weiss, W. W. 2000, Baltic Astronomy, 9, 590 3
Lambert, D. L. 1993, Physica Scripta Volume T, 47, 186 2, 5
Lind, K., Asplund, M., & Barklem, P. S. 2009, A&A, 503, 541 2
Lind, K., Asplund, M., Barklem, P. S., & Belyaev, A. K. 2011, A&A, 528, A103 2, 9
Mashonkina, L. 2013, A&A, 550, A28 1, 8, 9
Mashonkina, L. I., Shimanskaya, N. N., & Sakhibullin, N. A. 1996, Astronomy Reports, 40, 187 1
Mashonkina, L. J. 1996, in Astronomical Society of the Pacific Conference Series, Vol. 108, M.A.S.S., Model Atmospheres and Spectrum Synthesis, ed. S. J. Adelman, F. Kupka, & W. W. Weiss, 140 1
Mauas, P. J., Avrett, E. H., & Loeser, R. 1988, ApJ, 330, 1008 1, 4, 12
Merle, T. 2012, PhD thesis, Université de Nice Sophia-Antipolis, Observatoire de la Côte d'Azur, Laboratoire Lagrange 4
Merle, T., Thévenin, F., Pichon, B., & Bigot, L. 2011, MNRAS, 418, 863 1, 3, 8, 10
Merle, T., Thévenin, F., Pichon, B., & Bigot, L. 2012, VizieR Online Data Catalog, 741, 80863 8
Mucciarelli, A., Bellazzini, M., Ibata, R., et al. 2012, MNRAS, 426, 2889 1
Mucciarelli, A., Bellazzini, M., Merle, T., et al. 2015, ArXiv e-prints 1
Norris, J. E., Bessell, M. S., Yong, D., et al. 2013, ApJ, 762, 25 1
Przybilla, N., Butler, K., Becker, S. R., & Kudritzki, R. P. 2001, A&A, 369, 1009 1
Seaton, M. J. 1962a, Proceedings of the Physical Society, 79, 1105 3, 4, 5, 12
Seaton, M. J. 1962b, in Atomic and Molecular Processes, ed. D. R. Bates, 375–+ 4, 12
Shimanskaya, N. N., Mashonkina, L. I., & Sakhibullin, N. A. 2000, Astronomy Reports, 44, 530 1, 2
Steenbock, W. & Holweger, H. 1984, A&A, 130, 319 2
Sundqvist, J. O., Ryde, N., Harper, G. M., Kruger, A., & Richter, M. J. 2008, A&A, 486, 985 2
Zatsarinny, O., Bartschat, K., Gedeon, S., et al. 2009, Phys. Rev. A, 79, 052709 3, 4, 10, 12
Zhao, G., Butler, K., & Gehren, T. 1998, A&A, 333, 219 1
Zhao, G. & Gehren, T. 2000, A&A, 362, 1077 1

Appendix A: Collision data with electrons

Appendix B: Collisions data with H atoms

Temperature [K]	1000	2000	4000	6000	8000	10000	15000	20000
lower and upper states				QM $\Upsilon^{e}_{ij}(T)$				
Allowed transitions								
3s ^{1}S - 3p ^{1}P	3.74e−02	9.64e−02	2.96e−01	5.98e−01	9.92e−01	1.47e+00	3.06e+00	5.21e+00
3p ^{3}P - 4s ^{3}S	2.02e−03	8.64e−03	3.89e−02	9.75e−02	1.91e−01	3.24e−01	8.58e−01	1.70e+00
3p ^{1}P - 4s ^{1}S	2.22e−01	6.32e−01	1.64e+00	2.86e+00	4.33e+00	6.06e+00	1.15e+01	1.85e+01
3p ^{1}P - 3d ^{1}D	1.95e−01	4.73e−01	1.20e+00	2.15e+00	3.33e+00	4.73e+00	9.20e+00	1.50e+01
4s ^{3}S - 4p ^{3}P [a]			4.57e+01	6.15e+01	8.14e+01			
Intercombination transitions (but with a log gf)								
3s ^{1}S - 3p ^{3}P	9.78e−02	3.09e−01	9.00e−01	1.58e+00	2.28e+00	2.97e+00	4.59e+00	6.04e+00
3s ^{1}S - 4p ^{3}P	1.91e−02	4.15e−02	8.85e−02	1.35e−01	1.80e−01	2.23e−01	3.27e−01	4.27e−01
3p ^{3}P - 4s ^{1}S	3.87e−02	9.97e−02	2.32e−01	3.61e−01	4.82e−01	5.96e−01	8.53e−01	1.07e+00
3p ^{3}P - 3d ^{1}D	6.55e−02	1.56e−01	3.60e−01	5.91e−01	8.41e−01	1.11e+00	1.82e+00	2.60e+00
4s ^{1}S - 4p ^{3}P	2.48e−01	4.82e−01	8.39e−01	1.11e+00	1.32e+00	1.51e+00	1.92e+00	2.27e+00
3d ^{1}D - 4p ^{3}P	1.77e−01	4.98e−01	1.38e+00	2.35e+00	3.30e+00	4.19e+00	6.21e+00	7.96e+00
Forbidden transitions								
3s ^{1}S - 4s ^{3}S	6.55e−03	2.05e−02	5.69e−02	9.56e−02	1.33e−01	1.70e−01	2.54e−01	3.30e−01
3s ^{1}S - 4s ^{1}S	3.81e−03	1.62e−02	4.93e−02	8.54e−02	1.23e−01	1.62e−01	2.69e−01	3.91e−01
3s ^{1}S - 3d ^{1}D	1.20e−02	3.03e−02	7.26e−02	1.24e−01	1.85e−01	2.58e−01	4.95e−01	8.18e−01
3p ^{3}P - 3p ^{1}P	8.45e−02	2.02e−01	5.43e−01	9.82e−01	1.47e+00	1.98e+00	3.26e+00	4.53e+00
3p ^{3}P - 4p ^{3}P [b]				2.05e-03				
3p ^{1}P - 4s ^{3}S	9.94e−02	2.63e−01	6.29e−01	9.79e−01	1.29e+00	1.58e+00	2.19e+00	2.70e+00
3p ^{1}P - 4p ^{3}P	1.89e−01	4.25e−01	9.23e−01	1.41e+00	1.88e+00	2.31e+00	3.27e+00	4.08e+00
4s ^{3}S - 4s ^{1}S	2.85e−02	6.84e−02	1.89e−01	3.36e−01	4.92e−01	6.52e−01	1.06e+00	1.46e+00
4s ^{3}S - 3d ^{1}D	2.76e−01	6.33e−01	1.35e+00	1.99e+00	2.56e+00	3.07e+00	4.13e+00	5.00e+00
4s ^{1}S - 3d ^{1}D	6.62e−02	1.64e−01	4.61e−01	8.76e−01	1.39e+00	1.98e+00	3.82e+00	6.17e+00
lower and upper states				SC $\Upsilon^{e}_{ij}(T)$				
Allowed transitions								
3s ^{1}S - 3p ^{1}P	3.59e+00	3.78e+00	4.17e+00	4.57e+00	4.98e+00	5.38e+00	6.42e+00	7.46e+00
3p ^{3}P - 4s ^{3}S	7.85e+00	8.86e+00	1.08e+01	1.26e+01	1.43e+01	1.59e+01	1.95e+01	2.28e+01
3p ^{1}P - 4s ^{1}S	7.42e+00	9.40e+00	1.30e+01	1.62e+01	1.91e+01	2.16e+01	2.71e+01	3.15e+01
3p ^{1}P - 3d ^{1}D	4.75e+00	5.98e+00	8.41e+00	1.07e+01	1.28e+01	1.48e+01	1.92e+01	2.30e+01
4s ^{3}S - 4p ^{3}P	2.87e+01	3.97e+01	6.03e+01	8.04e+01	1.00e+02	1.19e+02	1.62e+02	2.01e+02
Intercombination transitions (but with a log gf)								
3s ^{1}S - 3p ^{3}P	7.82e−06	8.89e−06	1.10e−05	1.31e−05	1.52e−05	1.71e−05	2.16e−05	2.56e−05
3s ^{1}S - 4p ^{3}P	3.72e−08	4.11e−08	4.94e−08	5.84e−08	6.79e−08	7.78e−08	1.04e−07	1.30e−07
3p ^{3}P - 4s ^{1}S	7.68e−06	9.48e−06	1.36e−05	1.81e−05	2.28e−05	2.76e−05	3.95e−05	5.12e−05
3p ^{3}P - 3d ^{1}D	4.36e−06	5.35e−06	7.63e−06	1.02e−05	1.30e−05	1.58e−05	2.31e−05	3.05e−05
4s ^{1}S - 4p ^{3}P	8.61e−08	6.44e−07	4.03e−06	1.03e−05	1.90e−05	2.94e−05	6.02e−05	9.51e−05
3d ^{1}D - 4p ^{3}P	3.39e+01	5.13e+01	7.59e+01	9.19e+01	1.06e+02	1.15e+02	1.31e+02	1.43e+02
Forbidden transitions								
3s ^{1}S - 4s ^{3}S	1.00e+00	1.00e+00	1.00e+00	1.00e+00	1.00e+00	1.00e+00	1.00e+00	1.00e+00
3s ^{1}S - 4s ^{1}S	1.00e+00	1.00e+00	1.00e+00	1.00e+00	1.00e+00	1.00e+00	1.00e+00	1.00e+00
3s ^{1}S - 3d ^{1}D	1.00e+00	1.00e+00	1.00e+00	1.00e+00	1.00e+00	1.00e+00	1.00e+00	1.00e+00
3p ^{3}P - 3p ^{1}P	1.00e+00	1.00e+00	1.00e+00	1.00e+00	1.00e+00	1.00e+00	1.00e+00	1.00e+00
3p ^{3}P - 4p ^{3}P	1.00e+00	1.00e+00	1.00e+00	1.00e+00	1.00e+00	1.00e+00	1.00e+00	1.00e+00
3p ^{1}P - 4s ^{3}S	1.00e+00	1.00e+00	1.00e+00	1.00e+00	1.00e+00	1.00e+00	1.00e+00	1.00e+00
3p ^{1}P - 4p ^{3}P	1.00e+00	1.00e+00	1.00e+00	1.00e+00	1.00e+00	1.00e+00	1.00e+00	1.00e+00
4s ^{3}S - 4s ^{1}S	1.00e+00	1.00e+00	1.00e+00	1.00e+00	1.00e+00	1.00e+00	1.00e+00	1.00e+00
4s ^{3}S - 3d ^{1}D	1.00e+00	1.00e+00	1.00e+00	1.00e+00	1.00e+00	1.00e+00	1.00e+00	1.00e+00
4s ^{1}S - 3d ^{1}D	1.00e+00	1.00e+00	1.00e+00	1.00e+00	1.00e+00	1.00e+00	1.00e+00	1.00e+00
Effective collision strength for ionization								
3s ^{1}S - 3s ^{2}S	5.36e−03	1.07e−02	2.15e−02	3.22e−02	4.29e−02	5.36e−02	8.05e−02	1.07e−01
3p ^{3}P - 3s ^{2}S	4.33e−01	8.65e−01	1.73e+00	2.60e+00	3.46e+00	4.33e+00	6.49e+00	8.65e+00
3p ^{1}P - 3s ^{2}S	1.05e+00	2.10e+00	4.21e+00	6.31e+00	8.42e+00	1.05e+01	1.58e+01	2.10e+01
4s ^{3}S - 3s ^{2}S	8.32e−03	1.66e−02	3.33e−02	4.99e−02	6.65e−02	8.32e−02	1.25e−01	1.66e−01
4s ^{1}S - 3s ^{2}S	2.73e−03	5.47e−03	1.09e−02	1.64e−02	2.19e−02	2.73e−02	4.10e−02	5.47e−02
3d ^{1}D - 3s ^{2}S	1.28e+00	2.55e+00	5.11e+00	7.66e+00	1.02e+01	1.28e+01	1.92e+01	2.55e+01
4p ^{3}P - 3s ^{2}S	1.96e+00	3.91e+00	7.82e+00	1.17e+01	1.56e+01	1.96e+01	2.93e+01	3.91e+01

[a] at 3000, 5000 and 7000 K from Mauas et al. (1988)
[b] at 5000 K from Mauas et al. (1988)

Table A.1. Effective collision strengths with electrons. Upper table: Quantum Mechanical (QM) data inferred from Zatsarinny et al. (2009) and unpublished data, excepted for 2 transitions we used data from Mauas et al. (1988). Lower table: Semi Classical (SC) data inferred from Seaton (1962a,b). For clarity, the 3s electron is omitted in the electronic configuration of each level.

Temperature [K]	500	1000	2000	4000	6000	8000	10000	15000	20000
lower and upper states	QM $\Upsilon_{ij}^{\rm H}(T)$								
Allowed transitions									
3s ^{1}S - 3p ^{1}P	3.66e−06		6.30e−06	9.89e−06	1.53e−05	2.33e−05			
3p ^{3}P - 4s ^{3}S	2.15e−01		2.59e−01	2.52e−01	2.52e−01	2.56e−01			
3p ^{1}P - 4s ^{1}S	8.40e−02		1.34e−01	1.49e−01	1.61e−01	1.77e−01			
3p ^{1}P - 3d ^{1}D	2.55e−02		3.80e−02	4.90e−02	6.15e−02	7.73e−02			
4s ^{3}S - 4p ^{3}P	9.21e−02		1.35e−01	1.78e−01	2.18e−01	2.56e−01			
Intercombination transitions									
3s ^{1}S - 3p ^{3}P	2.95e−06		5.34e−06	1.38e−05	3.31e−05	7.15e−05			
3s ^{1}S - 4p ^{3}P	3.19e−05		3.84e−05	4.38e−05	4.95e−05	5.64e−05			
3p ^{3}P - 4s ^{1}S	1.12e−01		1.61e−01	1.52e−01	1.45e−01	1.46e−01			
3p ^{3}P - 3d ^{1}D	1.27e−01		9.56e−02	8.29e−02	8.12e−02	8.17e−02			
4s ^{1}S - 4p ^{3}P	2.41e−02		1.14e−01	2.09e−01	2.91e−01	3.65e−01			
3d ^{1}D - 4p ^{3}P	1.50e−01		6.36e−01	1.22e+00	1.72e+00	2.19e+00			
Forbidden transitions									
3s ^{1}S - 4s ^{3}S	3.23e−05		4.22e−05	4.96e−05	6.22e−05	7.74e−05			
3s ^{1}S - 4s ^{1}S	2.78e−05		4.17e−05	4.58e−05	5.46e−05	7.15e−05			
3s ^{1}S - 3d ^{1}D	4.00e−05		3.28e−05	3.50e−05	4.29e−05	5.24e−05			
3p ^{3}P - 3p ^{1}P	5.96e−02		8.53e−02	1.01e−01	1.14e−01	1.27e−01			
3p ^{3}P - 4p ^{3}P	7.51e−02		8.81e−02	8.56e−02	8.10e−02	7.59e−02			
3p ^{1}P - 4s ^{3}S	1.95e−01		3.30e−01	4.26e−01	5.34e−01	6.69e−01			
3p ^{1}P - 4p ^{3}P	2.41e−02		4.54e−02	5.51e−02	6.16e−02	6.91e−02			
4s ^{3}S - 4s ^{1}S	1.20e−01		2.24e−01	3.00e−01	3.65e−01	4.34e−01			
4s ^{3}S - 3d ^{1}D	2.88e−02		4.56e−02	6.72e−02	1.02e−01	1.44e−01			
4s ^{1}S - 3d ^{1}D	3.05e−01		9.42e−01	1.16e+00	1.26e+00	1.33e+00			
Effective collision strength for charge exchange process (Mg I + H $\Longleftrightarrow$ Mg II + H$^-$)									
3s ^{1}S - 3s ^{2}S	2.72e−05		4.73e−05	7.60e−05	1.08e−04	1.41e−04			
3p ^{3}P - 3s ^{2}S	1.72e−02		4.11e−02	7.60e−02	1.03e−01	1.24e−01			
3p ^{1}P - 3s ^{2}S	1.68e−01		1.75e−01	2.46e−01	3.42e−01	4.35e−01			
4s ^{3}S - 3s ^{2}S	1.03e+00		1.19e+00	1.41e+00	1.68e+00	1.99e+00			
4s ^{1}S - 3s ^{2}S	1.37e+01		1.69e+01	1.92e+01	2.10e+01	2.27e+01			
3d ^{1}D - 3s ^{2}S	5.59e+00		6.68e+00	7.38e+00	8.00e+00	8.57e+00			
4p ^{3}P - 3s ^{2}S	1.53e+00		1.89e+00	2.09e+00	2.27e+00	2.43e+00			

lower and upper states	CL $\Upsilon_{ij}^{\rm H}(T)$							
Allowed transitions								
3s ^{1}S - 3p ^{1}P	9.30e−03	1.93e−02	4.15e−02	6.65e−02	9.43e−02	1.25e−01	2.14e−01	3.21e−01
3p ^{3}P - 4s ^{3}S	1.95e−02	4.17e−02	9.39e−02	1.57e−01	2.29e−01	3.13e−01	5.68e−01	8.89e−01
3p ^{1}P - 4s ^{1}S	4.93e−02	1.13e−01	2.81e−01	5.05e−01	7.85e−01	1.12e+00	2.20e+00	3.64e+00
3p ^{1}P - 3d ^{1}D	4.93e−02	1.13e−01	2.81e−01	5.05e−01	7.85e−01	1.12e+00	2.20e+00	3.64e+00
4s ^{3}S - 4p ^{3}P	6.37e−01	1.49e+00	3.86e+00	7.11e+00	1.13e+01	1.63e+01	3.26e+01	5.46e+01
Intercombination transitions (but with a log gf)								
3s ^{1}S - 3p ^{3}P	2.67e−08	5.67e−08	1.26e−07	2.08e−07	3.03e−07	4.11e−07	7.37e−07	1.14e−06
3s ^{1}S - 4p ^{3}P	2.65e−10	5.46e−10	1.15e−09	1.82e−09	2.54e−09	3.33e−09	5.55e−09	8.15e−09
3p ^{3}P - 4s ^{1}S	1.34e−07	2.85e−07	6.34e−07	1.05e−06	1.53e−06	2.07e−06	3.72e−06	5.76e−06
3p ^{3}P - 3d ^{1}D	9.24e−08	1.95e−07	4.29e−07	7.03e−07	1.02e−06	1.37e−06	2.43e−06	3.73e−06
4s ^{1}S - 4p ^{3}P	5.16e−06	1.28e−05	3.56e−05	6.85e−05	1.11e−04	1.64e−04	3.40e−04	5.79e−04
3d ^{1}D - 4p ^{3}P	1.02e+00	3.05e+00	1.01e+01	2.12e+01	3.62e+01	5.53e+01	1.20e+02	2.10e+02
Effective collision strength for ionization (Mg I + H $\Longleftrightarrow$ Mg II + H + e$^-$)								
3s ^{1}S - 3s ^{2}S	1.59e−03	3.24e−03	6.77e−03	1.06e−02	1.47e−02	1.90e−02	3.12e−02	4.50e−02
3p ^{3}P - 3s ^{2}S	3.48e−02	7.19e−02	1.53e−01	2.44e−01	3.43e−01	4.53e−02	7.68e−01	1.14e+00
3p ^{1}P - 3s ^{2}S	2.63e−02	5.52e−02	1.21e−01	1.97e−01	2.83e−01	3.80e−01	6.68e−01	1.02e+00
4s ^{3}S - 3s ^{2}S	4.51e−02	9.60e−02	2.15e−01	3.57e−01	5.22e−01	7.09e−01	1.28e+00	1.99e+00
4s ^{1}S - 3s ^{2}S	1.93e−02	4.12e−02	9.34e−02	1.57e−01	2.31e−01	3.16e−01	5.76e−01	9.05e−01
3d ^{1}D - 3s ^{2}S	1.38e−01	2.99e−01	6.91e−01	1.17e+00	1.75e+00	2.42e+00	4.49e+00	7.14e+00
4p ^{3}P - 3s ^{2}S	3.06e−01	6.68e−01	1.56e+00	2.68e+00	4.02e+00	5.58e+00	1.05e+01	1.68e+01

Table B.1. Effective collision strengths with H atoms. Upper table: Quantum Mechanical (QM) data inferred from Barklem et al. (2012). Lower table: Classical (CL) data inferred from Drawin (1969). For clarity, the 3s electron is omitted in the electronic configuration of each level.